Exchange stiffness, magnetization, and spin waves in cubic and hexagonal phases of cobalt

X. Liu, M. M. Steiner, and R. Sooryakumar
Department of Physics, The Ohio State University, Columbus, Ohio 43210

G. A. Prinz
Naval Research Laboratory, Washington, DC, 20375

R. F. C. Farrow and G. Harp*
IBM Almaden Research Center, San Jose, California 95120

(Received 10 October 1995)

We utilize Brillouin light scattering to investigate the magnetic properties of the hexagonal-close-packed as well as the body- and face-centered cubic phases of elemental cobalt stabilized as thin epilayers. Expressions for the dependence of the surface and bulk magnons on applied magnetic field and in-plane propagation direction yield the exchange stiffness constant D, saturation magnetization M, and magnetic anisotropy fields of the cobalt atoms synthesized in these distinct crystal structures. Estimates of D and M are also calculated from the electronic band structure for the different crystalline phases. Satisfactory agreement is found between theory and experiment. The implications of these results towards our understanding of magnetic properties of itinerant ferromagnets are discussed.

INTRODUCTION

Recent advances in molecular beam epitaxy (MBE) methods have enabled growth of different (stable as well as metastable) phases of given atomic species in thin film geometries.[1,2] The synthesis usually relies on special growth procedures that secure the desired crystalline order to an underlying substrate template surface. The availability of different structural phases of a specific material becomes especially valuable in the case of ferromagnetic metals, since the energy difference between two distinct crystal structures is often comparable to energies associated with magnetic effects.[3] The 3*d* transition metals Fe, Co, and Ni are particularly interesting in this regard. They are relatively simple ferromagnets that can be stabilized in different crystal structures, and their magnetic properties are largely determined by well-localized 3*d* orbitals lying mainly within the Wigner-Seitz (WS) sphere whose radii are comparable to interatomic spacings. Thus structural order in these elemental ferromagnets can be expected to influence magnetic and configurational energies in important ways, with magnetism playing an important role in determining the ground-state crystal structure. Because of this interplay between bonding and magnetism, the transition-metal ferromagnets are also excellent model systems to test current electronic structure calculations, especially those that compare the magnetic properties of a given atom in different crystalline environments.

The very existence of local magnetic moments in transition metals indicates that the interaction between itinerant electrons is complicated. Thus, even when acting predominantly delocalized, correlation effects among the *d* electrons should not be overlooked. Within a Stoner model for itinerant magnetism, a spin magnetic moment develops if the gain in exchange energy is larger than the loss in kinetic energy. In the case of 3*d* ferromagnets, this magnetization per unit volume (M) leads to a nearly filled set of majority 3*d* bands, while the minority 3*d* band is partially filled.[4] The exchange splitting in bulk hcp Co, for instance, is 1 eV, yielding a spin magnetic moment of $1.57\mu_B$.[5] The exchange stiffness constant (D), which is related to the spin susceptibility $\chi(q,\omega)$, determines the long-wavelength low-frequency magnon dispersion $\hbar\omega = Dq^2$. D is hence another important quantity that is a direct measure of the stability of the magnetic phase.[6] Magnetic anisotropies (surface and volume contributions), which determine how the energy of the system varies when the direction of M changes, also play crucial roles in stabilizing long-range ferromagnetic order in laminar geometries.[7]

In this study we focus on cobalt since it is the only 3*d* transition-metal element to be stabilized in the naturally occurring hexagonal-close-packed phase as well as in face- and body-centered-cubic configurations. The thin-film geometry in which such phases are available is especially attractive for investigating their magnetic excitations through Brillouin light scattering since the quantized wave vector normal to the film moves the bulk magnon well into the exchange regime. We exploit this technique to determine important magnetic parameters (D, M, and anisotropies) of the three phases of cobalt. Since for small momentum and energy the spin susceptibility $\chi(q,\omega)$ is dominated by the spin-wave pole, the exchange stiffness constant can be calculated rigorously from knowledge of the spin-dependent band structure.[6] Moreover, the imaginary part of $\chi(q,\omega)$ is observed by light scattering from spin waves. We determine theoretical estimates for D from self-consistent local density approximation (LDA) solution of a linearized muffin-tin-orbital (LMTO) band structure calculation.[5] The density functional calculations within the LDA also provide results for the magnetic moment for each of the three phases, thus allowing comparison to measured values of these parameters in the three crys-

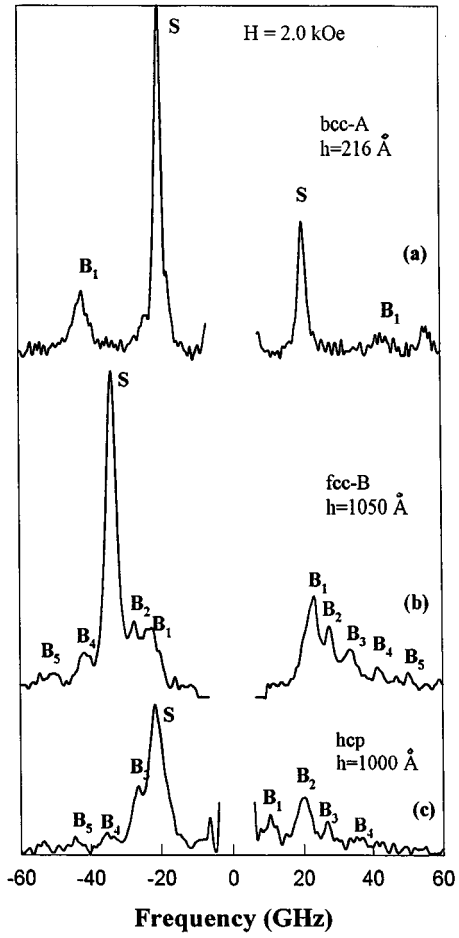

FIG. 1. Brillouin spectra at room temperature from (100) bcc, (110) fcc, and (0001) hcp cobalt films at an angle of incidence of 40° in a field of 2 kOe. The label S identifies the surface magnon and B_n the quantized bulk magnons. The thickness of each film (h) is identified.

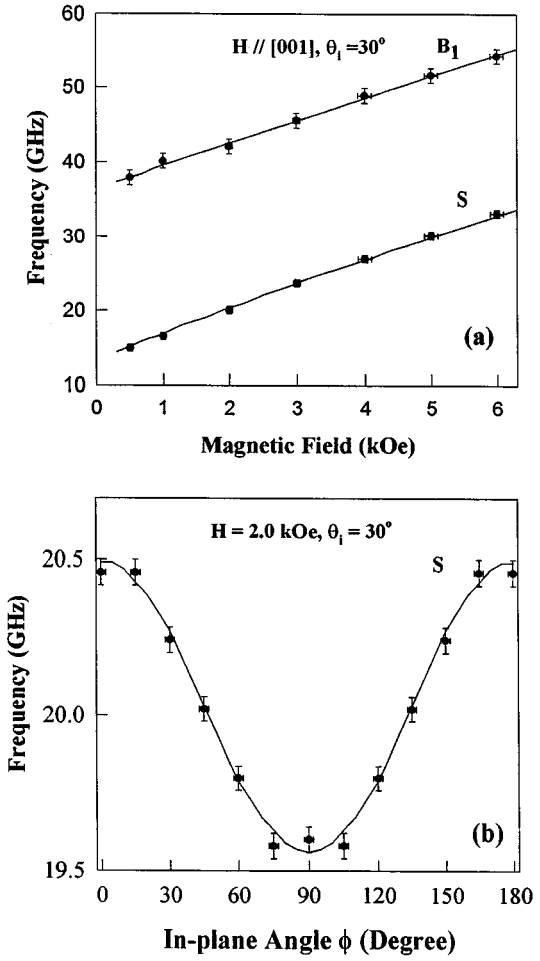

FIG. 2. (a) Magnetic field dependence of the surface (ω_S) and bulk (ω_{B1}) magnon frequencies in the (100)-oriented bcc cobalt film bcc-A. (b) In-plane magnon dispersion with ϕ being the in-plane angle between [001] direction and the external magnetic field. The solid lines through the data are a fit utilizing parameters discussed in the text.

talline phases. We find good agreement between theory and experiment.

EXPERIMENTAL DETAILS

Several single crystalline Co films were grown by MBE methods, and the different phases were stabilized via growth on specific substrates and buffer layers as described in detail in Refs. 1,2. Two bcc cobalt films of different orientations were grown. One of these films, labeled bcc-A, was (100) oriented and 216 Å thick, while the second film, bcc-B, was (110) with a thickness of 202 Å. Both films were grown on GaAs substrates.[1] The two fcc films, fcc-A and fcc-B, were, respectively, 1150-Å-thick [(110) orientation] and 1050-Å-thick [(100) orientation] films grown on a sequence of designed (primarily Cu, Ag, and Pt) seed layers.[2] The 1000-Å-thick film of (0001) hcp Co was stabilized on 100 Å Cu(111) deposited on 10 Å Pt(111) on basal plane sapphire.[2] The structure of each epilayer was confirmed through x-ray diffraction,[2] while surface-enhanced x-ray-absorption fine-structure (EXAFS) studies[8] were also used to establish the bcc structure. The average magnetic moment of the films was measured at room temperature with a superconducting quantum interference device (SQUID) magnetometer. The Brillouin measurements were performed at room temperature using a six-pass tandem Fabry-Pérot interferometer in a backscattering geometry.[9] P-polarized light of about 100 mW in a single-mode 5145-Å laser line was focused onto the samples with a typical sampling time of about 2 h. The angle of incidence, θ_i, of the incident photons, measured to an accuracy of $\pm 2°$, was set between 20° and 40°. The spin-wave excitations were analyzed in the depolarized configuration in order to suppress phonon signals. In our Brillouin measurements, **q**, the in-plane magnon wave vector, was always perpendicular to the applied magnetic field H, which lay parallel to the plane of the film.

Since the magnon frequencies are dependent on the exchange as well as anisotropy fields, the magnetic field as well as directional dependence of the surface and bulk magnons was determined.[10] Two independent light scattering experiments were thus carried out on each sample. In the first, the sample was rotated in finite steps about the film normal such that **q** systematically lay along different in-plane directions; a constant magnetic field of 1.5 or 2.0 kOe was applied. In

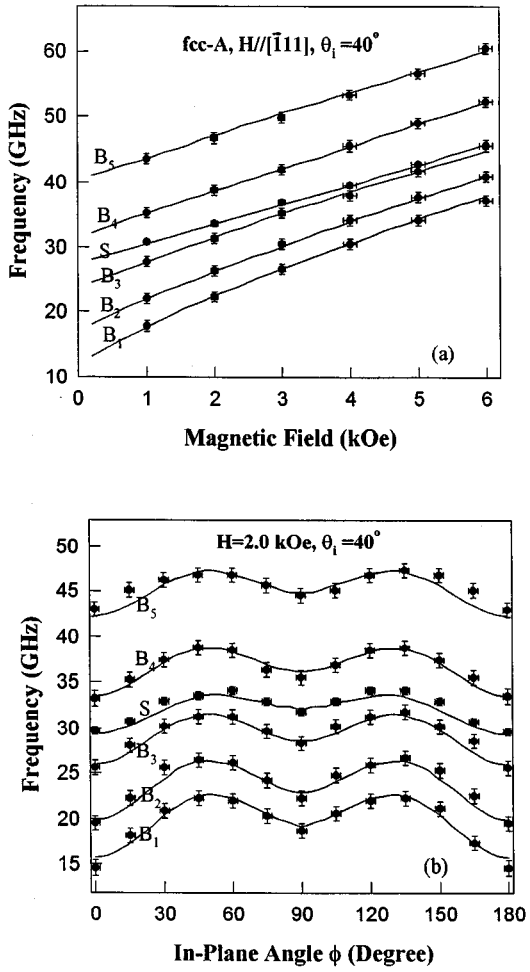

FIG. 3. (a) Magnetic field dependence of the surface (ω_S) and bulk (ω_{B1-5}) magnon frequencies in the (110)-oriented fcc cobalt film. (b) In-plane magnon dispersion with ϕ being the in-plane angle between [001] direction and the external magnetic field. The solid lines through the data are a fit utilizing parameters discussed in the text.

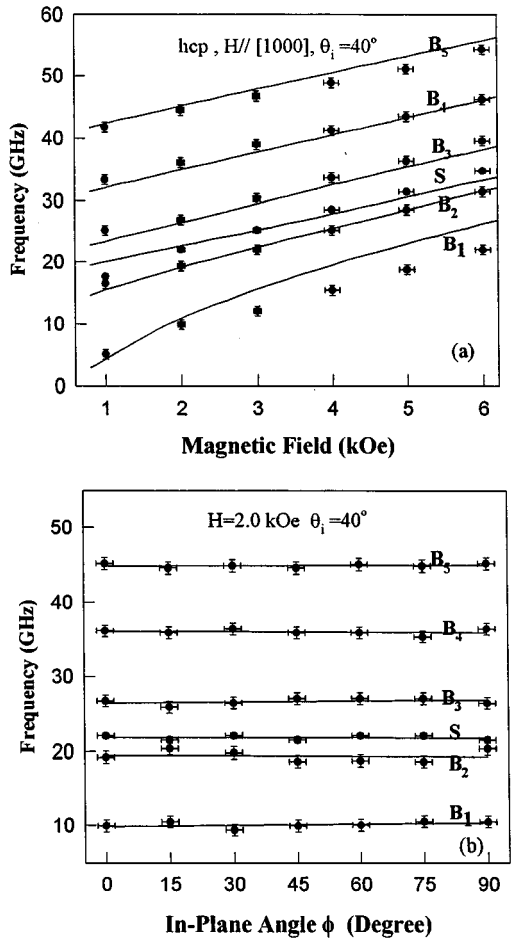

FIG. 4. (a) Magnetic field dependence of the surface (ω_S) and bulk (ω_{B1-5}) magnon frequencies in the (0001) oriented hcp cobalt film. (b) In-plane magnon dispersion with ϕ being the in-plane angle between [1000] direction and the external magnetic field. The solid lines through the data are a fit utilizing parameters discussed in the text.

this case the frequencies (ω_S, ω_B) of the surface and bulk spin waves were determined at each propagation direction. In the second experiment, the magnetic field was aligned along one of the crystalline axis ([001] for bcc (100) Co, [110] for bcc (110), [011] for fcc (100), [111] for fcc (110) Co, and [1000] for hcp Co). The magnon frequencies were measured as a function of H in this geometry for each film.

RESULTS

Typical Brillouin spectra of spin waves from films of the bcc, fcc, and hcp phases are shown in Fig. 1 for an applied field of 2.0 kOe. Figure 1(a) shows a spectrum from the 216-Å (001)-oriented sample bcc-A. The surface (S) and $n=1$ bulk (B_1) magnons are clearly observed. Figures 1(b) and 1(c) show corresponding modes from fcc-B and hcp Co films. Being thicker ($\sim$ 1000 Å) than the bcc epilayer, the Brillouin spectra from the fcc and hcp films reveal several bulk magnons ($n=1$, 2, 3, 4, and 5). Figures 2(a) and 2(b) summarize the field and inplane directional dependence of ω_S and ω_{B1} in film bcc-A. Here ϕ is defined as the in-plane angle between H and the crystallographic [001] direction for the bcc and fcc films, and [1000] direction for the hcp film. Since in the thin-film geometry the bulk magnon frequencies are dominated by the exchange interaction, the difference between the frequencies of B_1 and S in Fig. 2(a) is particularly sensitive to the exchange stiffness constant D, while the slope of the curves controls the gyromagnetic ratio (γ). The approximately 1-GHz difference in the frequency of S between $\phi=0$ and 90° in Fig. 2(b) indicates the presence of a weak uniaxial anisotropy contribution to the surface magnon dispersion in this bcc cobalt epilayer. The solid curves through the data in Fig. 2 are fits based on the description presented below and were determined self-consistently by fitting the ω-vs-H and ω-vs-ϕ data in Figs. 2(a) and 2(b), respectively.

Figures 3(a) and 3(b) summarize the field and in-plane directional dependence of the magnon frequencies in the fcc-A Co film. The dispersion for this (110)-oriented fcc Co epilayer exhibits [Fig. 3(b)] an approximate fourfold symmetry with the data, revealing the two in-plane directions [001]

($\phi=0°$) and [$\bar{1}10$] ($\phi=90°$) being magnetically inequivalent with frequency differences of about 2 GHz along these directions. The data for the hcp structure [Figs. 4(a) and 4(b) are similar to that of fcc cobalt, although, within experimental uncertainty, no in-plane anisotropy is observed in this case in the magnon frequencies for varying directions of **q**. As in Fig. 2, the fits to the data from the fcc and hcp films were each determined self-consistently to fit the field and ϕ dependence of ω_S and ω_B. The results are shown as solid lines in Figs. 3 and 4.

The theory used to fit the Brillouin data has been discussed in detail in Refs. 11–16. The important fields contributing to the spin-wave frequencies are the magnetic anisotropies, dipolar exchange, and external applied field. Frequencies of the surface and bulk modes can be calculated for this ferromagnetic films including exchange interactions in a continuum limit that is valid for long-wavelength spin-wave excitations. The theory of dipole-exchange behavior invokes Maxwell's equation of magnetostatics and equations of motion for the time and spatially varying magnetization $\vec{m}$. These equations have the form

$$\frac{d}{dt}\vec{m}=\gamma(\vec{m}+\vec{M})\times(\vec{H}_{\rm eff}+\vec{h}_d), \tag{1}$$

where M is the static magnetization, γ the gyromagnetic ratio, and h_d is the dipolar magnetic field. The effective magnetic field $H_{\rm eff}$ contains the static magnetic field H, the exchange $[(D/M)\nabla^2\vec{m}]$, and anisotropy fields H_a that normally have contributions from magnetocrystalline, surface/interfacial, and magnetoelastic terms. The geometry for the spin-wave dispersion calculations was chosen so that the x axis lies normal to both film surfaces and the axis of saturation magnetization which was selected to lie along z. The anisotropy fields depend not only upon the specific crystal structure, but also on the orientation of the film. The components of $d\vec{m}/dt$ for the (100)-grown cubic film are

$$\frac{dm_x}{dt}=\gamma\left\{H+\left(\frac{2K_1}{M}\right)[1-2\sin^2(2\varphi)]+\left(\frac{2K_u}{M}\right)(1-2\sin^2\varphi)+Dk^2\right\}m_y-\gamma Mh_y, \tag{2a}$$

$$\frac{dm_y}{dt}=\gamma\left\{H+\left(\frac{2K_1}{M}\right)[1-\tfrac{1}{2}\sin^2(2\varphi)]+\left(\frac{2K_u}{M}\right)\cos^2\varphi+\left(\frac{2K_p}{M}\right)+Dk^2\right\}m_x+\gamma Mh_x, \tag{2b}$$

for (110)-grown cubic film

$$\frac{dm_x}{dt}=\gamma\left\{H+\left(\frac{2K_1}{M}\right)\{1-\tfrac{1}{2}[\sin^2\varphi+3\sin^2(2\varphi)]\}+\left(\frac{2K_u}{M}\right)(1-2\sin^2\varphi)+Dk^2\right\}m_y-\gamma Mh_y, \tag{3a}$$

$$\frac{dm_y}{dt}=-\gamma\left\{H+\left(\frac{2K_1}{M}\right)\{1-[2\sin^2\varphi+\tfrac{3}{8}\sin^2(2\varphi)]\}+\left(\frac{2K_u}{M}\right)\cos^2\varphi+\left(\frac{2K_p}{M}\right)+Dk^2\right\}m_x+\gamma Mh_x, \tag{3b}$$

and for (0001) hcp film

$$\frac{dm_x}{dt}=\gamma\left[H+\frac{36K_u}{M}\cos(6\varphi)+Dk^2\right]m_y-\gamma Mh_y, \tag{4a}$$

$$\frac{dm_y}{dt}=-\gamma\left[H-\frac{2K_1'}{M}+\left(\frac{6K_u}{M}\right)\cos(6\varphi)+Dk^2\right]m_x+\gamma Mh_x, \tag{4b}$$

where k is the wave vector of the spin waves. In the above equations, K_1 is the first-order fourfold magnetocrystalline anisotropy, and K_u and K_p are in- and out-of-plane uniaxial anisotropies respectively. K_1' is the first-order anisotropy constant of the hcp structure where the anisotropy energy density is given by $K_1\sin^2\theta$, where θ is the angle the magnetization makes with the hexagonal axis. In our convention, $K_u>0$ puts an in-plane easy axis along [001] for the bcc and fcc films and along [1000] for the hcp films. K_p is defined such that $2K_p/M+4\pi M<0$ for an out-of-plane easy axis. After linearization, the two coupled equations for $\vec{m}$ are solved together with general exchange boundary conditions[11] and the continuity of $h_y, b_x(=h_x+4\pi m_x)$ at $x=0$ and h, where h is the film thickness. A superposition of six solutions for m_i is required to satisfy these conditions.

The magnon branches of the spin-wave manifold obtained from such a treatment are the surface localized Damon-Eshbach excitation S and quantized bulk magnons B_n whose wave vector normal to the film surface is given approximately by $k_{Bn}=n(\pi/h)$, where $n=1,2,\ldots$. These modes are evident in Fig. 1 where S is characterized by the well-known asymmetry in Stokes–anti-Stokes ratio, while the bulk excitations correspond to magnons B_1–B_5 whose frequencies depend strongly on film thickness through k_{Bn}. The self-consistent fits to the field and directional dependent Brillouin data are shown as solid lines in Figs. 2–4, and the resulting parameters (exchange stiffness constant, magnetic moment, and anisotropic fields) are summarized in Table I. The values for the magnetization determined from fits to the Brillouin data are in good agreement with those measured directly with the SQUID magnetometer. The errors in exchange stiffness D and magnetic moment μ were each determined by fitting the experimental data within their error ranges, while other parameters were held constant.

We note that because of the presence of anisotropic fields in the thin films, the magnetization at low fields may not rotate uniformly with external magnetic field. In this case the direction of M needs to be determined consistently as an input parameter to the spin-wave frequency calculation. This is determined by minimizing the free energy with respect to the angle made by $\vec{M}$ and the easy axis. In our case, since the measurements were mostly carried out at fields at or above 1.0 kOe and the anisotropies were relatively weak, we found no significant difference in the fits to the Brillouin data be-

TABLE I. Magnetic parameters for the different Co films. D_{expt} [D_{calc}] and μ_{spin}/μ_B (expt) [$(\mu_{\text{spin}}/\mu_B)$ (calc)] are, respectively, the measured (calculated) values for the exchange constant and magnetic moment per unit volume. K_1, K_u, and K_p are the measured magnetocrystalline and in-plane and out-of-plane uniaxial anisotropies. An asterisk indicates that for the hcp film the magnetocrystalline constant is K_1'. γ is the gyromagnetic ratio.

	D_{expt} (meV Å^2)	D_{calc} (meV Å^2)	μ_{spin}/μ_b (expt)	μ_{spin}/μ_B (calc)	K_1 (10^5 erg/cm^3)	K_u (10^5 erg/cm^3)	K_p (10^5 erg/cm^3)	γ (GHz/kOe)
fcc Co(100)	466±16	808	1.68±0.06	1.66	−5.0±0.2	0.0±0.1	0.0±0.1	2.90±0.02
fcc Co(110)	466±16	808	1.68±0.06	1.66	−6.0±0.2	0.0±0.1	0.0±0.1	2.92±0.02
hcp Co(0001)	435±35	712	1.68±0.06	1.57	34*±4	0.0±0.1	NA[a]	2.60±0.02
bcc Co(110)	430±22	764	1.26±0.06	1.70	0.0±0.1	−6.2±0.5	8.0±0.5	2.80±0.02
bcc Co(100)	428±22	764	1.36±0.06	1.70	−0.2±0.1	−0.85±0.5	−3.6±0.1	2.80±0.02

[a]NA: nonapplicable.

tween those that consider such deviations of $\vec{M}$ and those where the magnetization tracks the external field.

Prior to discussing our results, we now describe theoretical estimates of the exchange stiffness D and the magnetization M. Our calculations are based on previous work by Edwards and Muniz[6] who determined an explicit formula for D within a multiband random-phase-approximation approach. Their result for D takes the form

$$(N_\uparrow - N_\downarrow)D = \frac{1}{3}\sum_{nk}\left[B_{n\downarrow}(k)N_{nk\downarrow} + B_{n\uparrow}(k)N_{nk\uparrow}\right] - \frac{1}{3}\sum_{mnk} C_{mn}(k)\frac{N_{nk\uparrow} - N_{mk\downarrow}}{E_{mk\downarrow} - E_{nk\uparrow}}, \tag{5}$$

where

$$B_{n\sigma}(k) = \frac{1}{2}\sum_{\mu\mu'}\left[\nabla^2 V_{\mu\mu'}(k)\right] a^*_{n\mu\sigma}(k) a_{n\mu',\sigma}(k),$$

$$C_{mn}(k) = \sum_\alpha |A^\alpha_{mn}(k)|^2, \tag{6}$$

with

$$A^\alpha_{mn}(k) = \sum_{\mu\mu'} \frac{\partial V_{\mu\mu'}(k)}{\partial k_\alpha} a^*_{m\mu\downarrow}(k) a_{n\mu',\uparrow}(k) \quad (\alpha = x,y,z). \tag{7}$$

Here $N_\uparrow$ and $N_\downarrow$ are the total number of electrons with spin-up and spin-down. $V_{\mu\mu'}(k)$ are the spin-independent Hamiltonian matrix elements between atomic orbitals μ,μ' Bloch states, $N_{nk\sigma}$ are the local density approximation (LDA) occupation number associated with band n, wave vector k, and spin σ, and the one-electron LDA energies $E_{nk\sigma}$ and $\alpha_{nk\sigma}$ are the eigenvalues and eigenvectors of the LDA equations

$$\sum_\nu H^\sigma_{\mu\nu}(k) a_{n\nu\sigma}(k) = E_{nk\sigma}(k) a_{n\mu\sigma}(k). \tag{8}$$

$H^\sigma_{\mu\nu}(k)$ is the spin-dependent Hamiltonian matrix elements. Both $H^\sigma_{\mu\nu}(k)$ and $V_{\mu\mu'}(k)$ were obtained from self-consistent band structure calculations. The band structures were calculated with the linear muffin-tin orbital within the atomic sphere approximation (LMTO-ASA) method with combined correction included and using the von Barth–Hedin parametrization of the exchange correlation potential.[5] Unlike previous studies,[6] we did not parametrize the paramagnetic bands to obtain the exchange splitting. Instead, spin-polarized calculations were used, resulting in more realistic exchange splittings. The advantage of our calculations is that there were no adjustable parameters. The lattice constants needed for the calculation for each of the crystalline phases were chosen to be 2.807 Å for bcc Co, 3.536 Å for fcc Co, and $a = 2.506$ Å and $c = 4.065$ Å for hcp Co, which are consistent with the measured values for these constants.[1,2] The band structure we determined for the three different phases of cobalt also permit their respective spin moments to be evaluated. The summation over k was carried out using the tetrahedral method.[5] In order to ensure convergence of all parameters involved in our calculations, we used up to 1015, 1012, and 954 k points in the irreducible Brillouin zone for the bcc, fcc, and hcp structures, respectively. The calculated values for D and M are summarized in Table I along with our experimental findings for these quantities and the magnetic anisotropies.

DISCUSSION

We first focus on the exchange stiffness D for the three phases of cobalt. Our experimental results establish approximately the same value of D of about 435 meV Å^2 for all three phases, thus indicating that D is largely insensitive to the lattice structure. This feature, namely, that the exchange stiffness of the Co films is not especially susceptible to the particular crystalline order, is also borne out in theoretical estimates of D which lie between 710 and 810 meV Å^2 for the three distinct crystal structures. Although the magnitudes of D that we calculate are larger than the measured stiffness in each of the phases, the theory does corroborate the experimental finding that D is not particularly influenced by the local crystal structure. The discrepancy between theory and experiment in the magnitude of D probably lies largely in the calculations. The main source of error is the extreme sensitivity of D to the exchange splitting δE_{ex} between majority

and minority bands.[6] We have found that a 1% modification in the exchange splitting leads to a 10% change in D. Errors in the theoretical estimates for $\delta E_{\rm ex}$ vary from 10% to 50% and are in large due to the neglect of dynamic correlation effects among electrons in the open 3d shell.[5] Accounting for such correlation effects is still a field of active research and beyond our present ability.

What are the implications of the insensitivity of D to local crystalline order in this 3d transition metal? In one extreme of the quantum theoretical description of magnetism, the localized model, each electron remains in the vicinity of an atom and the intra-atomic electron-electron interactions determine the magnetic moment. In the other extreme where the electrons are not bound to individual atoms, the collection of itinerant electrons interact with each other, leading to magnetic order. Experimental spin-wave spectra throughout this range have been observed. In the case of transition metals like cobalt, although the 3d electrons are spatially localized, itinerant models are found to be valid since the bandwidth is comparable to effective electron-electron interaction strength. If the Heisenberg description were valid, then in the local moment picture, one obtains an exchange constant $D=zJSr^2/\hbar\gamma$. Here, z is the number of nearest neighbors at a distance r possessing spin S coupled by an exchange J. Since the gyromagnetic ratio γ, S, and the nearest neighbor distances are very similar in the different phases, this leaves the only parameter which varies in going from fcc Co to hcp Co to bcc Co is the coordination number z. Hence, within the local moment picture, D should simply scale with z ($z_{\rm hcp}=z_{\rm fcc}=12$, $z_{\rm bcc}=8$), which is not found. While the details of the band structure depend strongly on the crystal structure, the summation over the whole Brillouin zone averages out these differences and the closeness of the final calculated results for D reflects the similarity of the overall electronic structure of the three phases. We therefore conclude that exchange stiffness in the 3d ferromagnet cobalt is well described by an itinerant description of magnetism with electron-electron correlations stabilizing the magnetic order.

In an earlier publication,[9] we reported on the exchange constant in a 357-Å bcc Co film, one of the thickest known bcc Co structures.[17] In this case the light scattering data yielded an exchange constant which was in fact approximately 2/3 (ratio of bcc to hcp coordination number) of the value of D in the bulk hcp phase, behavior consistent with a local moment ferromagnet. While it has not been possible to fabricate other bcc Co films of this thickness, thinner films ($\sim$ 200 Å) can, as in the present study, be readily produced. The fact that the two bcc films used in this study have different orientations and the result of our electronic structure calculations lend weight to our conclusion regarding the itinerant nature of the magnetism in cobalt.

Turning to the saturation magnetization M or, equivalently, the magnetic moment per unit volume, $\mu_{\rm spin}/\mu_B$, we find good agreement between theory and experiment (Table I for fcc cobalt. The agreement for bcc cobalt is, however, not as satisfactory with the measured value $\mu_{\rm spin}\approx 1.30\mu_B$, being smaller than the value $1.70\mu_B$ predicted from band structure calculations. We suspect that the reduction in the saturation magnetization in the bcc Co epilayers arises from migration of Ga and As from the GaAs substrate into the metal film. Evidence for a smaller average magnetic moment per atom in bcc cobalt films grown on GaAs has been previously reported from neutron scattering measurements.[18] In these experiments it was shown that M varied with depth within a 100-Å film with the segment near the metal/GaAs interface, acquiring a significantly depressed average moment per atom due to As poisoning of the epilayer. If a similar reduction occurs in our two 200-Å-thick bcc Co films, it would lead to an effective magnetization of about $1.35\mu_B$ averaged over the entire film; this moment agrees well with measurement. The measured value of $\mu_{\rm spin}$ ($1.71\ \mu_B$) of the hcp film is the same as in fcc Co and 8% larger than the calculated value. The overall good agreement between calculated and measured values of M in the fcc and hcp films therefore confirms earlier findings[5] that the LMTO-ASA method provides a satisfactory description of the many aspects of the electronic structure of the narrow-band Co epilayers stabilized in distinct crystalline phases.

While the magnitude of M is a measure of the *spin* magnetic moment in the Co films investigated (orbital moment is much smaller[19]), magnetic anisotropy determines how the energy of the system varies when the direction of M changes. The direction of (interface) induced anisotropies in ultrathin magnetic films is currently of special interest for applications in magneto-optical technologies. Contributions to the anisotropy normally stem from shape effects, local atomic environment (crystallinity) that arises from the spin-orbit interaction, and magnetoelastic effects which are especially relevant in supported thin films and overlayers.[20] For the relatively large thickness of our films, surface anisotropy contributions are negligible. The effective anisotropy energy thus primarily arises from demagnetization ($K_D=-2\pi M^2$ in thin films), magnetocrystalline (K_1), and magnetoelastic (K_{ME}) contributions.

Magnetoelastic effects depend on strains along particular crystallographic directions, the magnetoelastic tensor, and elastic constants of the film. For our hcp and fcc Co films whose film thickness are large (1000 Å), the strains are negligible and therefore magnetoelastic effects can be safely neglected. While strain can account for uniaxial anisotropies, the insignificant strains in the hcp and fcc films would suppress contributions from K_u and K_p indicated in Eqs. (2)–(4) if they are magnetoelastic in origin. This is evident in Table I where K_u and K_p are found to be zero for these films. On the other hand, the bcc Co films were stabilized to thicknesses of only about 200 Å. In this instance the predicted film-substrate lattice mismatch strain ($\sim$0.25%) is, though small, finite. It was recently shown[21] that, with elastic constants determined from phonon dispersion measurements on the same films, magnetoelastic interactions driven by lattice mismatch can give rise to uniaxial anisotropies K_u and K_p of the order given in Table I for the two bcc cobalt layers.

For the fcc films, the crystalline anisotropy constants K_1 determined from the Brillouin data are the same within the experimental error as those deduced from other experimental probes of the same Co films.[22] For the hcp film the crystalline anisotropy energy density is given by $K_1'\sin^2\theta$, where θ is the angle the magnetization makes with the hexagonal axis. The value of K_1' we have deduced from the (0001) hcp film is in good agreement with its value in Ref. 22. The lack of in-plane anisotropy in the Brillouin frequencies of the bulk and surface magnons in the hcp film [Fig. 4(b)] is con-

sistent with the high symmetry of the hexagonal (0001) atomic plane. The K_1's we have determined for the two bcc Co films used in our investigation are smaller than that given in Ref. 23. The smaller K_1 in our bcc-A sample was also confirmed by an independent ferromagnetic resonance (FMR) measurement of the same film. For bulk 3*d* transition metals, calculations of magnetic anisotropy often differ from measured values by orders of magnitude, occasionally even yielding the wrong sign.[20] We hence did not attempt to calculate the anisotropies.

CONCLUSIONS

In summary, we have carried out Brillouin light scattering measurements on thin films of the hexagonal and cubic phases of cobalt which have become available through advances in MBE-growth techniques. These experiments have provided for the exchange stiffness D, saturation magnetization M, and the anisotropy fields in the distinct crystal structures. Comparisons between measured values of D and M and those calculated from the electronic band structure of the fcc, hcp, and bcc phases using theoretical descriptions of dynamical spin fluctuations are found to be in satisfactory agreement. These results verify the itinerant nature of the 3*d* electrons known to be responsible for magnetism in these ferromagnets.

ACKNOWLEDGMENTS

Work at the Ohio State University was supported by the National Science Foundation under Grant No. DMR 93-03568 and that at NRL by the Office of Naval Research. Partial support for M.M. Steiner was provided by the Department of Energy, Basic Energy Sciences, Division of Material Sciences. We also acknowledge useful discussions with R.L. Stamps.

*Present address: Department of Physics and Astronomy, Ohio University, Athens, OH 45701.

[1] G. A. Prinz, Phys. Rev. Lett. **54**, 1051 (1985).
[2] (a) G. R. Harp, R. F. Farrow, D. Weller, T. A. Rabedeau, and R. F. Marks, Phys. Rev. B **48**, 17 538 (1993); (b) D. Weller, G. R. Harp, R. F. C. Farrow, A. Cebollada, and J. Sticht, Phys. Rev. Lett. **72**, 2097 (1994).
[3] V. L. Moruzzi, P. M. Marcus, K. Schwarz, and P. Mohn, Phys. Rev. B **34**, 1784 (1986).
[4] D. J. Singh, Phys. Rev. B **45**, 2258 (1992).
[5] M. M. Steiner, R. C. Albers, and L. J. Sham, Phys. Rev. B **45**, 13 272 (1992).
[6] D. M. Edwards and R. B. Muniz, J. Phys. F **15**, 2339 (1985).
[7] C. H. Lee, R. F. C. Farrow, C. J. Liu, E. E. Marinero, and C. J. Chien, Phys. Rev. B **42**, 11 384 (1990).
[8] Y. U. Idzerda, W. T. Elam, B. T. Jonker, and G. A. Prinz, Phys. Rev. Lett. **62**, 6120 (1991).
[9] J. Karanikas, R. Sooryakumar, B. Jonker, and G. A. Prinz, J. Appl. Phys. **69**, 6120 (1991).
[10] X. Liu, R. Sooryakumar, C. J. Gutierrez, and G. A. Prinz, J. Appl. Phys. **75**, 7021 (1994).
[11] R. E. Camley and D. L. Mills, Phys. Rev. B **18**, 4821 (1979).
[12] G. T. Rado and R. J. Hicken, J. Appl. Phys. **63**, 3885 (1988).
[13] B. Hillebrands, Phys. Rev. B **41**, 530 (1990).
[14] J. F. Cochran and J. R. Dutcher, J. Appl. Phys. **63**, 3814 (1988).
[15] G. Rupp, W. Wettling, R. S. Smith, and W. Jantz, J. Magn. Magn. Mater. **45**, 404 (1984).
[16] R. L. Stamps, Phys. Rev. B **49**, 339 (1994).
[17] A separate paper dealing with possible evidence for the presence of surface anisotropies and/or inhomogeneous internal fields in this particular 357-Å-thick bcc Co film is currently in preparation.
[18] J. A. C. Bland, R. D. Bateson, P. C. Riedi, R. G. Graham, H. J. Lauter, J. Penfold, and C. Shackleton, J. Appl. Phys. **69**, 4989 (1991).
[19] Per Söderlind, Olle Eriksson, Börje Johansson, R. C. Albers, and A. M. Boring, Phys. Rev. B **45**, 12 911 (1992).
[20] H. J. F. Jansen, Phys. Today **48**(4), 50 (1995).
[21] S. Subramanian, X. Liu, R. L. Stamps, R. Sooryakumar, and G. A. Prinz, Phys. Rev. B **52**, 1890 (1995).
[22] D. Weller, G. R. Harp, R. F. C. Farrow, A. Cebollada, and J. Sticht, Phys. Rev. Lett. **72**, 2097 (1994).
[23] C. J. Gutierrez, J. J. Krebs, and G. A. Prinz, Appl. Phys. Lett. **61**, 2476 (1992).